

# Substructures Revealed by the Sunyaev–Zel’dovich Effect at 150 GHz in the High Resolution Map of RX J1347–1145

Eiichiro KOMATSU,<sup>1 2</sup> Hiroshi MATSUO,<sup>3</sup> Tetsu KITAYAMA,<sup>4</sup> Makoto HATTORI,<sup>2</sup> Ryohei KAWABE,<sup>5</sup> Kotaro KOHNO,<sup>5</sup> Nario KUNO,<sup>5</sup> Sabine SCHINDLER,<sup>6</sup> Yasushi SUTO,<sup>7 8</sup> and Kohji YOSHIKAWA<sup>9</sup>

<sup>1</sup>*Department of Astrophysical Sciences, Princeton University, Princeton, NJ 08544, USA*  
*E-mail(EK): komatsu@astro.princeton.edu*

<sup>2</sup>*Astronomical Institute, Tôhoku University, Aoba, Sendai 980-8578*

<sup>3</sup>*National Astronomical Observatory, Mitaka, Tokyo 181-8588*

<sup>4</sup>*Department of Physics, Tokyo Metropolitan University, Hachioji, Tokyo 192-0397*

<sup>5</sup>*Nobeyama Radio Observatory, Minamimaki, Minamisaku, Nagano 384-1305*

<sup>6</sup>*Astrophysical Research Institute, Liverpool John Moores University, Byrom Street, Liverpool, L3 3AF, England, UK*

<sup>7</sup>*Department of Physics, The University of Tokyo, Tokyo 113-0033*

<sup>8</sup>*Research Center for the Early Universe, School of Science, The University of Tokyo, Tokyo 113-0033*

<sup>9</sup>*Department of Astronomy, Kyoto University, Kyoto 606-8502*

(Received ; accepted )

## Abstract

We report on mapping observations toward the region of the most luminous X-ray cluster RX J1347–1145 ( $z = 0.45$ ) through the Sunyaev–Zel’dovich effect at 21 GHz and 150 GHz with the Nobeyama 45-m telescope. While a low angular resolution image at 21 GHz (beam-size  $\sigma_{\text{FWHM}}$  of  $76''$ ) shows a consistent feature with the ROSAT/HRI X-ray image, a higher angular resolution image ( $\sigma_{\text{FWHM}} = 13''$ ) at 150 GHz reveals complex morphological structures of the cluster region, which cannot be simply described by the spherical isothermal  $\beta$ -model. If such inhomogeneous morphological features prove to be generic for high redshift clusters, distance measurements to the clusters based on their Sunyaev–Zel’dovich data with low angular resolution imaging should be interpreted with caution.

**Key words:** cosmology: observations – distance scale – cosmic microwave background – galaxies: clusters: individual (RX J1347–1145) – X-rays: galaxies

## 1. Introduction

The multi-band observation of galaxy clusters up to  $z \sim 1$  provides a unique opportunity to reconstruct the clustering evolution, the cosmological parameters, and the peculiar velocity field on large scales (e.g., Bahcall 1988; Rephaeli 1995; Birkinshaw 1999). In particular, the recent mapping observations of clusters using the state-of-the-art interferometers (Carlstrom, Joy, Grego 1996; Carlstrom et al. 2000) are accumulating impressive *negative* intensity images in centimeter bands through the Sunyaev–Zel’dovich (SZ) effect (Zel’dovich, Sunyaev 1969). The most important cosmological application of such data is to estimate the global value of the Hubble constant,  $H_0$ . Although the SZ effect can be used as a potential standard candle, previous attempts to estimate  $H_0$  were not sufficiently accurate (e.g., Kobayashi, Sasaki, Suto 1996; Birkinshaw 1999). This is probably because they usually neglect the non-sphericity, substructure, and non-isothermal profile of the intra-cluster mat-

ter. Recent numerical simulations of clusters (e.g., Inagaki, Sugimoto, Suto 1995; Yoshikawa, Itoh, Suto 1998; Jing, Suto 2000) have shown that the departure from the spherical isothermal  $\beta$ -model is appreciable and that the inhomogeneous morphology is quite generic.

High angular resolution imaging through the SZ effect is essential in resolving detailed structure of clusters. In centimeter interferometric measurements, the beam-size of  $\sigma_{\text{FWHM}} \sim 100''$  is typical, and can be as small as  $\sim 40''$  (Carlstrom, Joy, Grego 1996), while the brightness sensitivity is degraded. In millimeter and submillimeter bands, on the other hand, the sensitive higher resolution imaging is now feasible with bolometer array detectors. This observing technique has been successfully applied to the brightest X-ray cluster RX J1347–1145 ( $z = 0.451 \pm 0.003$ ) at 350 GHz with  $\sigma_{\text{FWHM}} = 15''$  (Komatsu et al. 1999), and subsequently at 143 GHz with  $\sigma_{\text{FWHM}} = 23''$  (Pointecouteau et al. 1999).

The bolometric X-ray luminosity of this cluster is exceptionally high,  $L_X h_{50}^2 = 2 \times 10^{46} \text{ erg s}^{-1}$  (Schindler

et al. 1997), where  $h_{50}$  is the Hubble constant in units of  $50 \text{ km s}^{-1} \text{ Mpc}^{-1}$ . Throughout this *Letter*, we use  $\Omega_0 = 1$  and  $\lambda_0 = 0$  for simplicity. The ASCA observation implies that the emission-weighted temperature is  $k_B T_e = 9.3_{-1.0}^{+1.1} \text{ keV}$  (Schindler et al. 1997). Applying the spherical isothermal  $\beta$ -model to the latest ROSAT/HRI data, we obtain the central electron number density,  $n_{e0} h_{50}^{-1/2} = 0.093 \pm 0.004 \text{ cm}^{-3}$ , the core radius,  $\theta_c = 8''.4 \pm 1''.0$ , and  $\beta = 0.57 \pm 0.02$ , where quoted errors are 90% confidence levels. The total mass inferred from the hydrostatic equilibrium is  $M(< 2 h_{50}^{-1} \text{ Mpc}) = 1 \times 10^{15} h_{50}^{-1} M_\odot$ . This cluster does not follow the temperature–luminosity relation because of the extremely high luminosity (Schindler 1999), and is known to be the strong cooling-flow cluster (Schindler et al. 1997; Allen, Fabian 1998). In this sense, this cluster may not be typical, but is an interesting target to be studied in detail individually.

The above two attempts to map the cluster using the SZ effect are not sensitive enough to resolve detailed structures; the former data (Komatsu et al. 1999) are very noisy because of the bad weather condition, and the latter (Pointecouteau et al. 1999) mapped only the central narrow stripe of the cluster. Therefore, as a part of the multi-band observing project of RX J1347–1145, we carried out the SZ mapping observation of the cluster at 21 GHz and 150 GHz with the Nobeyama 45-m telescope. In this *Letter*, we report on the complex morphological structures detected in the 150 GHz map with the unprecedented angular resolution ( $\sigma_{\text{FWHM}} = 13''$ ), which can hardly be identified from the lower resolution map at 21 GHz ( $\sigma_{\text{FWHM}} = 76''$ ). This demonstrates the importance of the high angular resolution imaging of clusters through the SZ effect.

## 2. The Sunyaev–Zel’dovich Mapping Observations with the Nobeyama 45-m telescope

### 2.1. Centimeter Mapping at 21 GHz

Mapping observations at 21 GHz were carried out during February 16–27 and April 14–22, 2000, in a raster-scan mode using the dual-polarization HEMT amplifier mounted on the Nobeyama 45-m telescope. In total, 9 scans were performed along the two orthogonal directions and each scan was separated by  $40''$  yielding the final field-of-view of  $6' \times 6'$ . A reference beam position was set to be  $400''$  away from a main beam, and the beam-size  $\sigma_{\text{FWHM}} = 76''.5$  was estimated by observing 3C279. The beam is accurately fitted to a Gaussian. The exposure time amounts to 31.2 ksec in February and 32.1 ksec in April. System noise temperatures were typically 135 K in February and 185 K in April. We calibrated the primary flux using 3C286 ( $2.56 \pm 0.02 \text{ Jy}$ ; Ott et al. 1994). The stability of antenna efficiency was tracked by moni-

toring the pointing source (1334–127), and we found that an rms variation in peak flux was 2% in February and 3% in April. A pointing offset is negligible compared with the beam-size.

We subtracted the low frequency scanning-noise from the map on the basis of the PLAITS method (Emerson, Gräve 1988) with a scale-length half the scan-length. The resulting  $1\sigma$  noise-levels in images are  $1.3 \text{ mJy beam}^{-1}$  in February and  $1.7 \text{ mJy beam}^{-1}$  in April. Combining the February and April runs, the final image achieves the noise-level of  $0.9 \text{ mJy beam}^{-1}$ . An absolute calibration error is 1%, which is dominated by the flux error of the primary calibrator 3C286.

### 2.2. Millimeter Mapping at 150 GHz

The higher angular resolution mapping of the cluster was performed with the Nobeyama Bolometer Array (NOBA; Kuno et al. 1993) on March 16 (20 ksec) and April 15 (8.5 ksec), 1999, as well as during February 16–27, 2000 (52.7 ksec). The total integration time is 81.2 ksec. NOBA consists of seven bolometers in hexagonal pattern with their band-passes centered at 150 GHz and bandwidths of 30 GHz. Bolometers are read-out through six differential circuits between a central bolometer and the other six surrounding ones. Fluctuations in atmospheric emissions are subtracted in real time by the readout electronics. The beam switching, or the sky chopping, is not used. The observation of this cluster was made with raster scans. A position angle of the array to the scan direction is  $19^\circ 1'$ . A single raster scan yields seven scan paths separated by  $5''.3$  each, and an observing stripe of  $37''.1$  in width. Three stripes thus cover the field-of-view of  $1'.9 \times 1'.9$  in right ascension and declination. Image restoration is performed using the six differential signals.

At the beginning and the end of each observing day, an elevation scan was made to measure the atmospheric transparency. The measured zenith optical depths at 150 GHz were 0.094–0.15 and 0.065–0.098 in our 1999 and 2000 runs, respectively. These scan data were also used to correct different sensitivities among bolometers. The pointing observation was made every 0.5 to 1 hour depending on the weather condition. The variation of the pointing is usually within  $3''$ . The data taken under strong wind conditions are discarded because of the unstable pointing and the degraded antenna efficiency. We calibrated the primary flux using the Mars in 1999, and K3–50A and OH5.89–0.39 in 2000. The flux of the Mars was obtained with the FLUXES procedure in the STAR-LINK package, and we employed  $6.5 \pm 0.2 \text{ Jy}$  (Sandell 1994) and  $8.8 \pm 0.9 \text{ Jy}$  (Falcke et al. 1998) for the fluxes of K3–50A and OH5.89–0.39, respectively. The beam pattern was measured using 3C279 which yields  $\sigma_{\text{FWHM}} = 12''.5$  and  $13''.2$  in 1999 and 2000, respectively.

An uncertainty of the beam-size is as large as  $1''$ . The beam is slightly elongated along the elevation direction by  $\sim 10\%$ , and the side-lobe level amounts to 3% of the peak value whereas the Gaussian yields 1% of the peak value. The pointing and gain stabilities were checked using 1334-127, and the rms variations in the peak fluxes were 12% in 1999 and 14% in 2000. These variations are largely ascribed to strong elevation-dependence of the antenna efficiency at 150 GHz. Correcting this gain variation, we estimate the total absolute calibration error to be 11% (7% in 1999 and 14% in 2000). The larger error in 2000 is due to the fact that the flux of 1334-127 daily changed up to  $\sim 20\%$  probably because of the burst, while it was stable in 1999 run.

Spike noises above the  $4\sigma$  level appearing in time-ordered data were removed. Again the map was created using the PLAIT method; the  $1\sigma$  noise-level in the final image is  $1.6 \text{ mJy beam}^{-1}$  ( $2.4 \text{ mJy beam}^{-1}$  in 1999, and  $2.1 \text{ mJy beam}^{-1}$  in 2000). In the final map, an averaged flux at the edge of map ( $64''$  away from the center),  $0.50 \pm 0.15 \text{ mJy beam}^{-1}$ , was subtracted to define the zero-level of the data.

### 3. Results

#### 3.1. Low Angular Resolution Image at 21 GHz

Figure 1(a) displays the final map of RX J1347–1145 at 21 GHz, which shows a bright point source near the center of the cluster. To estimate the accurate position and the flux at 21 GHz, we observed the source with VLA at 8.46 GHz (18 ksec) on May 16, 1999, and at 22.46 GHz (3.6 ksec) on May 20, 1999. Measured fluxes are  $22.42 \pm 0.04 \text{ mJy}$  at 8.46 GHz and  $11.55 \pm 0.17 \text{ mJy}$  at 22.46 GHz. Since the VLA configuration is insensitive to the SZ effect, these values accurately measure the central radio source flux. The derived source position is ( $13^{\text{h}}47^{\text{m}}30^{\text{s}}.622 \pm 0^{\text{s}}.0005$ ,  $-11^{\circ}45'09''.44 \pm 0''.009$ ), and precisely coincides with that of the optical center of the central cD galaxy. Although the X-ray peak position from the ROSAT/HRI data is offset from the optical center (Schindler et al. 1997), this offset is smaller than the nominal pointing uncertainty of ROSAT/HRI. In the following discussion, therefore, the X-ray peak position is assumed to coincide with the optical center and the central radio source position.

In total, we have three datasets at 21 GHz taken in three years: March 1998 (Komatsu et al. 1999), March 1999 (unpublished), and February and April, 2000 (this paper). The 1998 and 1999 runs were done in the cross-scan mode. We have measured central peak-intensities of  $8.6 \pm 2.0 \text{ mJy beam}^{-1}$  in 1998,  $7.8 \pm 1.2 \text{ mJy beam}^{-1}$  in 1999, and  $8.3 \pm 0.9 \text{ mJy beam}^{-1}$  in 2000. These results show no significant time variation of the source flux value during the past two years, and the averaged peak-

intensity is  $8.2 \pm 0.7 \text{ mJy beam}^{-1}$ .

Figure 1(b) plots the 21 GHz map after subtracting the contribution of the point source, adopting the VLA flux at 22.46 GHz. Its overall shape around the central part is fairly similar to that of the X-ray surface brightness contours overlaid in white solid lines, supporting the SZ interpretation over the entire cluster scale. The resulting central intensity (smoothed over the beam-size) of the SZ decrement relative to the edge of map ( $200''$  away from the center) is  $I_{\text{SZ}}(0) = -3.3 \pm 0.9 \text{ mJy beam}^{-1}$ , or equivalently,  $\Delta T_{\text{RJ}}(0) = -1.6 \pm 0.4 \text{ mK}$  in terms of the Rayleigh–Jeans brightness temperature decrement. Deconvolving the beam-pattern by approximating the cluster profile with the spherical isothermal  $\beta$ -model with the ROSAT/HRI best-fit values for  $\theta_c$  and  $\beta$  (§1), we obtain the central  $y$ -parameter,  $y(0) = (7.8 \pm 2.1) \times 10^{-4}$  (relative to the edge of map). Moreover, if we average the measured peak-intensities over the datasets taken in three years, we obtain  $y(0) = (7.7 \pm 1.6) \times 10^{-4}$ .

Our  $y(0)$  agrees very well with the value expected from the X-ray best-fit parameters,  $y(0)h_{50}^{1/2} = 8.0 \times 10^{-4}$ , if the SZ effect is negligible at the edge of map. Note that Komatsu et al. (1999) possibly overestimated the SZ intensity at the cluster center by  $1.75 \text{ mJy beam}^{-1}$ , as they used the central source flux of  $13.3 \text{ mJy}$  at 21 GHz on the basis of the power-law interpolation of the spectrum at 1.4, 28.5, and 100 GHz. We now realize that it is not a good approximation.

#### 3.2. High Angular Resolution Image at 150 GHz

Figure 1(c) shows the image at 150 GHz smoothed with a Gaussian filter so that the effective beam-size becomes  $20''.6$  (the  $1\sigma$  noise-level is  $1.3 \text{ mJy beam}^{-1}$ ). Although the central point source is fainter at 150 GHz than at 21 GHz, it still affects the diffuse negative intensity field around the center to some extent. The most remarkable feature in this image is a strong negative intensity region located  $\sim 20''$  south-east from the center. The peak intensity in this region is  $-5.4 \text{ mJy beam}^{-1}$  relative to the edge of map. This value is  $4.2\sigma$  significance level, and 2.5 times larger than that expected from the spherical isothermal  $\beta$ -model,  $I_{\text{SZ}}(\Delta\theta = 20'') \sim -2 \text{ mJy beam}^{-1}$ .

In the following, we quantify the statistical significance of the detection of this negative excess emission. As shown in figure 2, we divide the data into four regions: south-east (SE), south-west (SW), north-east (NE), and north-west (NW). The central region is excluded so as to remove the contamination of the point source. Then we evaluate fluxes in those regions. The results are summarized in table 1 together with the  $1\sigma$  error of  $2.0 \text{ mJy}$  each. The mean flux averaged over all regions is  $-6.4 \pm 1.0 \text{ mJy}$ , and thus the detection of the SZ decrement at 150 GHz is  $6.4\sigma$  level. The reality of the negative excess in the SE region is supported by the fol-

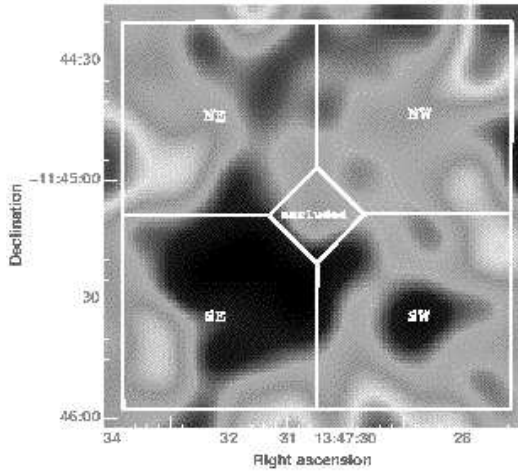


Fig. 2.. The definition of regions (see section 3.2).

lowing facts; (i) the fluxes of the other three regions are consistent with each other within the  $1\sigma$  level, (ii) relative to the mean flux over the other three regions,  $\bar{F} = -4.7 \pm 1.15$  mJy, the excess flux in the SE region is  $F_{SE} - \bar{F} = -6.6 \pm 2.3$  mJy, corresponding to  $2.9\sigma$  significance, and (iii) the excess in the SE region is persistent both in 1999 and in 2000. Thus we interpret this negative excess flux being due to the enhanced SZ effect.

To further explore the significance of this excess, let us consider the residual map after subtracting the SZ signal assuming the spherical isothermal  $\beta$ -model. For this purpose, we employ the best fit radial profile from the ROSAT/HRI data, and the emission-weighted temperature, 9.3 keV, measured with ASCA (§1). We refer to this as model L (low temperature). After convolving the model image with the effective beam and correcting for the zero-level, we subtract this from the observed map. Then we find that the model L implies a central radio source flux of  $3.8 \pm 1.3$  mJy, and the expected flux in each region is  $-5.1$  mJy. The latter value is consistent with those listed in table 1 except for the SE region where the difference is  $3.1\sigma$ . This is also consistent with the mean flux, indicating that the global feature of the SZ effect at 150 GHz is consistent with model L as well as at 21 GHz. Figure 1(d) shows the 150 GHz map after subtracting the central source flux of 3.8 mJy. While the X-ray contours overlaid in the figure seem to trace the detected SZ enhancement to some extent, the X-ray flux in the SE region is much smaller than that expected from the excess SZ flux we detected at 150 GHz.

In summary, we conclude that we detect an inhomogeneous morphology of the SZ signal toward the cluster at 150 GHz. The angular scale of the negative excess is around  $40''$ , and thus cannot be resolved in the lower angular resolution image at 21 GHz.

Table 1. Fluxes in four regions toward RX J1347–1145 (see figure 2 for the definition). Models L and H represent the expected fluxes from the spherical isothermal  $\beta$  model with temperatures of  $k_B T_e = 9.3$  keV and 16.2 keV, respectively.

	flux [mJy]
SE (south-east) .....	$-11.3 \pm 2.0$
NE (north-east) .....	$-4.7 \pm 2.0$
NW (north-west) .....	$-3.3 \pm 2.0$
SW (south-west) .....	$-6.1 \pm 2.0$
mean .....	$-6.4 \pm 1.0$
model L (9.3 keV) .....	$-5.1$
model H (16.2 keV) .....	$-8.8$

#### 4. Comparison with Previous Work

Using the IRAM/Diablo bolometer array, Pointecouteau et al. (1999) found that the peak position of the SZ decrement at 143 GHz is offset to the east of the X-ray peak position. Since they scanned in a narrow strip ( $30''$  in declination and  $120''$  in right ascension) along west-east direction whose width is comparable to the beam-size ( $\sigma_{FWHM} = 23''$ ), the resulting map is insensitive to the offset in north-south direction. Thus their result does not contradict our finding on the image basis. They presented a different interpretation for this negative enhancement; they assume that the offset between the X-ray peak position and the radio source position is real, and ascribe the offset between the SZ and the X-ray peak positions to the contamination of the positive radio source embedding in the SZ decrement tracing the X-ray signal. More specifically, they found the best-fit values for the central  $y$ -parameter,  $y(0) = 12.7^{+2.9}_{-3.1} \times 10^{-4}$ , and for the central point source flux,  $6.1^{+4.3}_{-4.8}$  mJy, at 143 GHz, adopting the  $\beta$ -model radial profile from the X-ray data. This  $y(0)$  corresponds to the much higher temperature of 16.2 keV than the ASCA value. We call this set of parameters model H (high temperature). When subtracting the SZ flux of the model H from our map at 150 GHz, we find the central source flux of  $6.6 \pm 1.3$  mJy. Since this value is close to their fit, our data at 150 GHz are consistent with their data, apart from the interpretation.

Here we compare our data to theirs quantitatively. (i) Taking into account the relativistic correction to the SZ effect (Itoh, Kohyama, Nozawa 1998) to extrapolate their  $y(0)$  at 143 GHz into the value at 21 GHz, model H predicts  $y(0) = 13.9^{+3.2}_{-3.4} \times 10^{-4}$  at 21 GHz. This value significantly exceeds our observed value,  $(7.7 \pm 1.6) \times 10^{-4}$ , which is well consistent with model L. (ii) Model H predicts the flux of  $-8.8$  mJy for each region defined in figure 2, which is systematically smaller than our observed values listed in table 1. Therefore, we conclude that model L with the excess SZ effect is more consistent with our data at 21 GHz and 150 GHz data than

model H. Their higher value of  $y(0)$  than ours is probably because of their narrower field-of-view. The excess SZ effect detected in the SE region would dominate the mean signal in their map, resulting in an overestimate of  $y(0)$ .

Incidentally the negative flux in the SE region at 150 GHz should show up as a *positive* SZ flux of 11 mJy in the JCMT/SCUBA band (350 GHz). While Komatsu et al. (1999) did not identify the corresponding peak in their SCUBA map, this is not inconsistent one another because of the high noise-level in their SCUBA map ( $1\sigma = 8$  mJy beam $^{-1}$ ).

## 5. Discussion

Possible physical explanations for the origin of the excess SZ feature include a) a projection contamination of another higher redshift cluster, b) warm gas associated with large-scale filamental structures, c) a substructure in the cluster gas, d) a cooling flow around the central region, and e) non-gravitational heating from AGNs and/or supernovae. Actually any explanation needs to be somewhat contrived, as it should be simultaneously consistent with the fairly smooth X-ray brightness distribution. Specifically, a) requires that the background cluster should be at  $z > 3$ , b) is viable only if the low temperature ( $\sim 0.4$  keV) gas extends over 1 Gpc along the line of sight, c) implies that the temperature of the substructure is larger than 200 keV, and d) and e) indicate that either pressure or virial equilibrium of the intracluster gas should be abandoned. Thus none of those possibilities seems to be sufficiently satisfactory.

Nevertheless if the complex morphological structure is generic to other high redshift clusters, distance measurements to the clusters based on the SZ data should be interpreted with caution. To elucidate this, let us consider how the enhanced decrement region at 150 GHz systematically affects the estimate of the Hubble constant from the 21 GHz data. The excess SZ flux at 21 GHz in the SE region is expected as  $-0.43$  mJy, based on the deviation from model L at 150 GHz in the same region ( $-6.2$  mJy). Since the extent of the SE region is smaller than the beam-area at 21 GHz, this flux amounts to 13% of  $I_{\text{SZ}}(0)$  at 21 GHz. This corresponds to overestimating  $I_{\text{SZ}}(0)$  relative to the isothermal  $\beta$ -model prediction, and thus to a systematic underestimate of  $H_0$  by 22% through the relation  $H_0 \propto I_{\text{SZ}}^{-2}(0)$ . This consideration might be relevant in understanding the Hubble diagram from the SZ effect (e.g., Kobayashi, Sasaki, Suto 1996; Birkinshaw 1999).

As demonstrated here, single-dish measurements of the SZ effect with high angular resolution play a complementary role to interferometers in exploring the intracluster gas state. In addition, a more accurate and higher resolution imaging observation in X-ray band with *Chandra*

and *XMM-Newton* observatories is important to understand the physical processes in this cluster as well as the future follow-up SZ observations including the SZ dedicated interferometers and JCMT/SCUBA.

We thank Akihiro Sakamoto and the NRO staff for their help during the observation at NRO, Izumi Ohta for observing RX J1347–1145 with NMA, and Wolfgang Reich for providing the data of OH5.89–0.39 and for useful comments on the data analysis. We also thank John Carlstrom, Uroš Seljak, and David N. Spergel for many valuable comments which have improved this *Letter*. E.K., T.K. and K.Y. acknowledge fellowships from Japan Society for the Promotion of Science. This research was supported in part by the Grants-in-Aid for the Center-of-Excellence (COE) Research of the Ministry of Education, Science, Sports, and Culture of Japan to RESCEU (No. 07CE2002), and Grand-in-Aid of the Ministry of Education, Sports, and Culture of Japan (No. 11440060).

## References

- Allen S.W., Fabian A.C. 1998, MNRAS 297, L57
- Bahcall N.A. 1988, ARA&A 26, 631
- Birkinshaw M. 1999, Phys. Rep. 310, 97
- Carlstrom J.E., Joy M.K., Grego L. 1996, ApJL 456, L75
- Carlstrom J.E., Joy M.K., Grego L., Holder G.P., Holzapfel W.L., Mohr J.J., Patel S., Reese E.D. 2000, Physica Scripta T85, 148
- Emerson D.T., Gräve R. 1988, A&A 190, 353
- Falcke H., Goss W.M., Matsuo H., Teuben P., Zhao J.H., Zylka R. 1998, ApJ 499, 731
- Inagaki Y., Sugimotohara T., Suto Y. 1995, PASJ 47, 411
- Itoh N., Kohyama Y., Nozawa S. 1998, ApJ 502, 7
- Jing Y.P., Suto Y. 2000, ApJL 529, L69
- Kobayashi S., Sasaki S., Suto Y. 1996, PASJ 48, L107
- Komatsu E., Kitayama T., Suto Y., Hattori M., Kawabe R., Matsuo H., Schindler S., Yoshikawa K. 1999, ApJL 516, L1
- Kuno N., Matsuo H., Mizumoto Y., Lange A.E., Beeman J.W., Haller E.E. 1993, Int. J. Infrared Millimeter Waves, 14, 749
- Ott M., Witzel A., Quirrenbach A., Krichbaum T.P., Standke K.J., Schalinski C.J., Hummel C.A. 1994, A&A 284, 331
- Pointecouteau E., Giard M., Benoit A., Désert F.X., Aghanim N., Coron N., Lamarre J.M., Delabrouille J. 1999, ApJL 519, L115
- Rephaeli . 1995, ARA&A 33, 541
- Sandell G. 1994, MNRAS 271, 75
- Schindler S., Hattori M., Neumann D.M., Böhringer H. 1997, A&A 317, 646
- Schindler S. 1999, A&A 349, 435
- Yoshikawa K., Itoh M., Suto Y. 1998, PASJ 50, 203
- Zel’dovich Ya.B., Sunyaev R.A. 1969, Ap&SS 4, 301

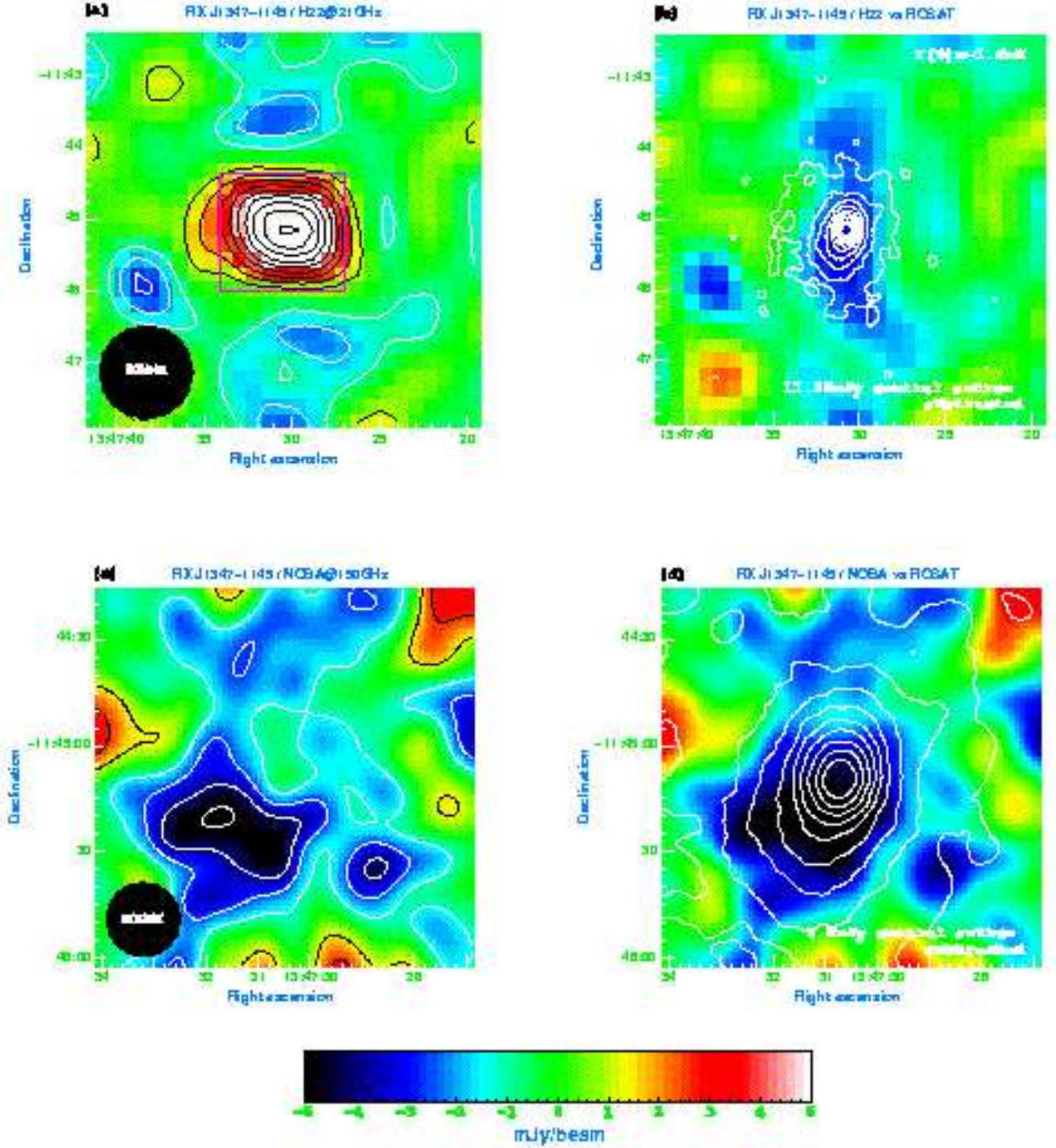


Fig. 1. The SZ maps of RX J1347–1145. (a) the 21 GHz map before subtracting the central point source. Field-of-view is  $6' \times 6'$  ( $2.4 h_{50}^{-1} \text{ Mpc} \times 2.4 h_{50}^{-1} \text{ Mpc}$ ). Black (white) lines represent  $1\sigma$  contours of positive (negative) intensities, where  $1\sigma = 0.9 \text{ mJy beam}^{-1}$ . The beam-size is shown as a filled black circle of a diameter  $76''5$ . The area defined by a magenta solid line corresponds to (c) and (d). (b) the 21 GHz map after subtracting the central point source. We used the VLA flux of  $11.55 \text{ mJy}$ . Overlaid in white lines are the X-ray contours, and represent 10–90% of the peak value in 10% intervals. The equivalent Rayleigh–Jeans temperature at the center is  $\Delta T_{\text{RJ}}(0) = -1.6 \pm 0.4 \text{ mK}$ . (c) the 150 GHz map before subtracting the central point source. Field-of-view is  $1'9 \times 1'9$  ( $0.75 h_{50}^{-1} \text{ Mpc} \times 0.75 h_{50}^{-1} \text{ Mpc}$ ). The lines have the same meaning as in the panel (a). In this panel, the beam-size is  $20''6$ , and  $1\sigma = 1.3 \text{ mJy beam}^{-1}$ . (d) the 150 GHz map after subtracting the central point source (assuming the flux of  $3.8 \text{ mJy}$ ) overlaid with the X-ray contours.